Journal of Sound and Vibration 399 (2017) 60–74

Contents lists available at ScienceDirect

Journal of Sound and Vibration

journal homepage: www.elsevier.com/locate/jsvi

Testing and performance of a new friction damper for seismic vibration control

Carlos A. Martínez, Oscar Curadelli *

Engineering Faculty, National University of Cuyo, CONICET, Mendoza, Argentina

ARTICLE INFO

Article history:
Received 13 October 2016
Received in revised form
4 March 2017
Accepted 19 March 2017
Handling Editor: A.V. Metrikine
Available online 28 March 2017

Keywords:
Friction damper
Passive vibration control
Energy dissipation

ABSTRACT

In the last two decades, great efforts were carried out to reduce the seismic demand on structures through the concept of energy dissipation instead of increasing the stiffness and strength. Several devices based on different energy dissipation principles have been developed and implemented worldwide, however, most of the dissipation devices are usually installed using diagonal braces, which entail certain drawbacks on apertures for circulation, lighting or ventilation and architectural or functional requirements often preclude this type of installations. In this work, a conceptual development of a novel energy dissipation device, called Multiple Friction Damper (MFD), is proposed and examined. To verify its characteristics and performance, the MFD was implemented on a single storey steel frame experimental model and tested under different conditions of normal force and real time acceleration records. Experimental results demonstrated that the new MFD constitutes an effective and reliable alternative to control the structural response in terms of displacement and acceleration. A mathematical formulation based on the Wen's model reflecting the nonlinear behaviour of the device is also presented.

1. Introduction

It is well known that, to reduce the structural response, external energy dissipation devices may be advantageously used. Friction dampers are often used in passive vibration control because they offer high energy dissipation capacity at relatively low cost and maintenance. Several friction devices have been tested and some of them have been implemented in buildings around the world [1].

Pall and Marsh [2] developed a friction damper known as the Pall frictional damper (PFD) in which the braces of an ordinary braced frame structure can slip in both directions by connecting the friction pads by four links at the intersection of the cross-braces. Anagnostides et al. [3] presented two new types of linear and rotational friction devices that are able to produce broad and stable hysteresis loops during an earthquake. Fitzgerald in 1989 [4] conducted a complete investigation on Slotted Bolted Connections (SBC) installed on braces, which dissipate energy through two friction steel surfaces in tension and compression loading cycles. Then, Grigorian et al. in 1993 [5] suggested to replace, in the SBC, the steel plates by brass plates. Sumitomo's friction damper [6] utilizes a more complicated design in which a pre-compressed internal spring exerts forces that are converted through the action of inner and outer wedges into a normal force on friction pads. Loo et al. [7] proposed a different type of symmetric connector for the SBC that eliminates the need for

* Corresponding author. Postal address: Facultad de Ingeniería. Centro Universitario, Parque Gral, San Martín CP 5500, Mendoza, Argentina.
E-mail address: ocuradelli@fing.uncu.edu.ar (O. Curadelli).

http://dx.doi.org/10.1016/j.jsv.2017.03.022
0022-460X/

shims which were considered expensive. Nims et al. [8] developed and tested a friction device called Energy Dissipating Restraint (EDR) that is similar to the Sumitomo's friction damper, except that the EDR utilizes steel and bronze friction wedges to convert the axial spring force into normal pressure on the cylinder. Mualla and Belev [9] proposed a friction damper device consisting of a central (vertical) plate, two side (horizontal) plates and two circular friction pad discs placed in between the steel plates, which are pin-connected, by braces to the frame. The energy dissipation occurs by the rotation of the central plate relative to the side plates when a horizontal deformation occurs in the frame. Cho and Kwon [10] developed a wall-type friction damper based on a Teflon slider to improve the seismic performance of reinforced concrete structures. Mirtaheri et al. [11] proposed an innovative friction damper called Cylindrical Friction Damper (CFD), which consists of two main parts, an inner shaft fitted inside an outer cylinder. Upon application of proper axial loading to both ends, the shaft moves inside the cylinder by overcoming the friction. This friction leads to considerable dissipation of mechanical energy. Khoo et al. [12] developed a self-centering sliding hinge joint that incorporates friction ring springs to improve the dynamic re-centering properties and reduce strength degradation, principally against major earthquakes. Later, Monir and Zeynali [13] presented a friction damper, which is assembled at the intersection of X-shaped diagonal braces. Recently, Samani et al. [14] presented the concept of a semi-active frictional damper called Adjustable Frictional Damper (AFD) in which the clamping force is secured by hydraulic pressure, which makes possible to control the seismic response of the structure by changing the clamping force of the dampers. The hysteretic behaviour of the AFD was studied numerically and good agreement with experimental results was found.

As regard to design procedures of friction energy dissipation systems, the following works may be included: Two design methodologies to determine systematically the quantity and the total slip force of friction damper–brace systems for elastic multi-storey building structures was presented by Filiatrault and Cherry [15] and Lee et al. [16]. Harmonic response of adjacent structures connected with a friction damper was studied by Bhaskararao and Jangid [17]. They observed that there exists an optimum slip force in the damper for which the peak displacement of a structure attains the minimum value, but the optimum slip force is different for each of the two connected structures. Park et al. [18] and Min et al. [19] presented new equivalent linearization techniques for a friction damper–brace system. Martinez et al. [20,21] proposed a robust and efficient design procedure to optimally define the energy dissipation capacity of added viscous and nonlinear hysteretic dampers on multiple-storey structures. Fallah and Honarparast [22] optimize the placement of type-Pall dampers through a genetic algorithm technique based on a multi-objective function. Performance of rotational friction dampers on frames of 3, 7 and 12 stories were studied by nonlinear time history dynamic analyses and evaluated experimentally by Mirzabagheri et al. [23]. Krack et al. [24] proposed a reliability based optimization of friction-damped systems using nonlinear modes, taking into account uncertainties in the friction coefficient, linear damping, and excitation level.

As specialized literature shows, traditional friction dampers are usually installed using diagonal braces, which entail certain drawbacks on apertures for circulation, lighting or ventilation and architectural or functional requirements often preclude this type of installations. Thus, this work presents a conceptual development of a novel energy dissipation device, called Multiple Friction Damper (MFD). This device, unlike traditional friction dampers, can be installed on any column without requiring major structural modifications. Another important feature of MFD is that the normal force necessary to attain the required friction force is applied through a preloading device resulting in a reduction of the axial force on the column where the MDF is installed. By means of experimental testing on a single-storey experimental model, the effectiveness on the structural response control, under different levels of normal force and characteristics of the excitation was assessed. A mathematical formulation based on the Wen's model describing the dynamical behaviour of the structure provided with the MFD is also presented.

2. Description of the Multiple Friction Damper (MFD)

The proposed friction damper consists of a set of friction elements stacked and coaxial with the column where it is installed (Fig. 1a). Each element is supported and assembled by two or four I-shaped steel plates that embrace the column to facilitate its installation (Fig. 1b). Both flanges (top and bottom) are provided with friction pads on which friction forces are generated during the relative motion between consecutive elements (slipping). Because of the axial symmetry, this type of connection enables the movement in any radial direction. Fig. 1c shows how the horizontal movement of the column is transmitted to each friction element through the toroidal ring connection. Indeed, when the column bends (elastic deformation), each toroidal ring clamped to it rotates freely inside the cylindrical bore and moves laterally pushing each friction element. Thus, the column transmits the lateral displacement, δ, to each friction element but, it does not transmit the rotation, θ. The relative displacement between contact friction pads generates friction forces.

The necessary normal force is adjusted by a preloading device (Fig. 1d), located at the top of the column. To ensure a correct operation of the MFD in slip phase, the normal force must not exceed the limit in which it might be prone to lock (stick phase). Thus, when the normal force is applied on the MFD, a reaction force against the roof (upper beam) is generated, and the axial force on the column is reduced because a fraction of the total initial axial force is taken by the stack of friction elements. The MFD can be installed on frames that undergo both, shear and bending deformations. In this latter case, it might be necessary the installation of a preloading device at each end of the column to absorb the small rotation of the beam-column join.

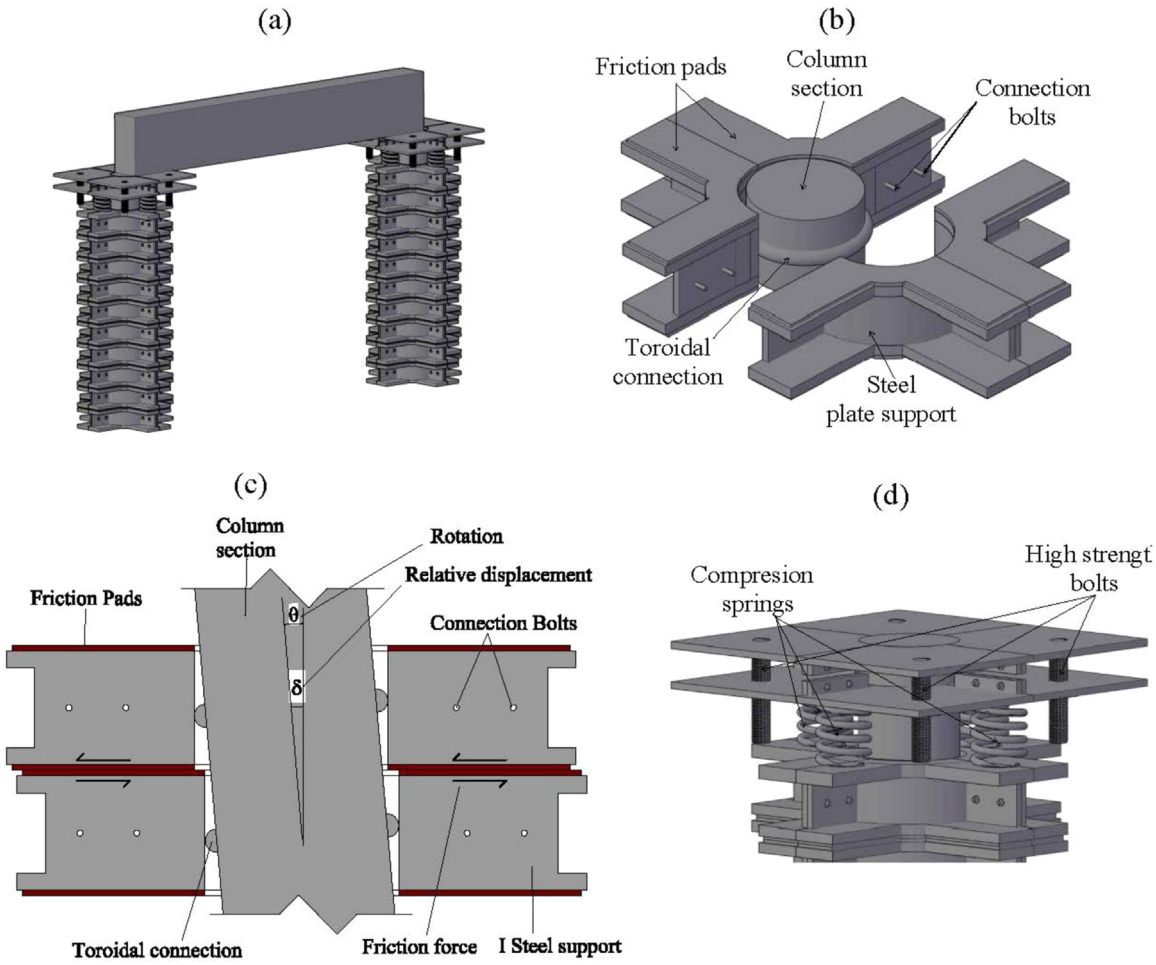

Fig. 1. a) Outline of MFD installed on a frame, b) Friction element, c) Contact between column and element, d) Preloading device.

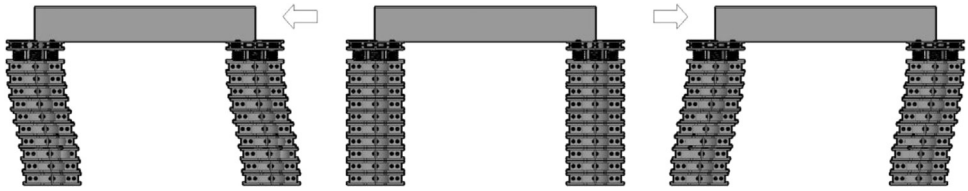

Fig. 2. Deformed configuration of a single-storey frame structure provided with the MFD.

Fig. 2 shows an overview of the deformed configuration of a single-storey frame. Thus, when the frame structure moves horizontally under lateral forces, relative displacements among friction elements produce friction forces on the interfaces, which dissipate energy and resist to the movement.

3. Experimental set-up

To characterize the properties of the MFD at different operating conditions and to assess the effectiveness in the control of structural response, a simple SDOF model was built and tested. The experimental program included: 1) Free vibration tests, 2) Data-collection of the hysteresis loops and 3) Forced vibration tests from different real acceleration records. Five levels of normal forces denoted by N=5, 10, 15 and 20% of total weight of the structure, W, were applied on the friction damper during the tests.

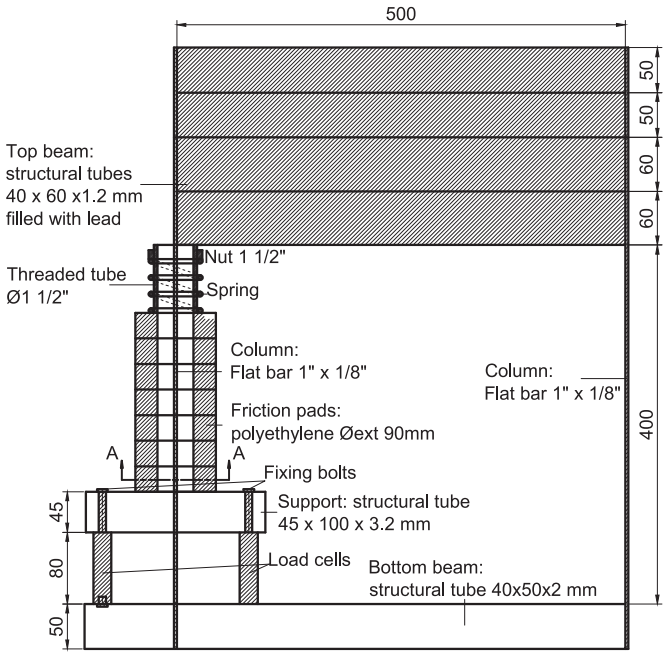

Fig. 3. Outline of the steel frame model provided with the MFD (dimensions in mm).

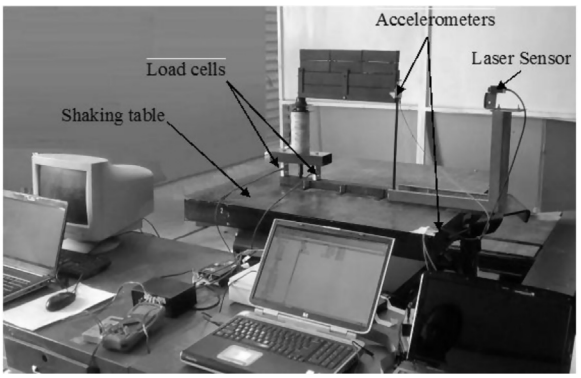

Fig. 4. Experimental setup and measuring system.

3.1. Experimental model

A single-storey, one-bay steel frame model was built under the premise that the fundamental frequency should be within the typical frequencies range of structures where dampers may be installed (0.5–2.0 Hz).

Overall dimensions of the frame model were chosen according to the available laboratory equipment (instrumentation, shaking table, etc.) (Fig. 3) resulting in a fundamental frequency of 1.74 Hz meeting the premise. The internal damping was measured to be 0.92% of the critical damping.

The required normal force (N=5, 10, 15 and 20% of total weight of the structure, W) was applied to the friction pads through a screw-compression spring device located at the top of the left column (Fig. 3).

3.2. Instrumentation

Fig. 4 shows the measuring setup used in experimental tests. The input ground motions were imposed on the model through a shaking table Moog 6DOF 2000E. A high-speed laser displacement sensor, Micro-epsilon opto NCDT 1607, was used to measure the horizontal displacement of the upper beam during dynamic and quasi-static tests. Acceleration records of the upper beam and the excitation imposed by the shaking table were measured by two PCB Piezotronics accelerometers (accel. max. 3 g, 700mV/g), sampled at 100 sps per channel. Normal forces were measured using two load cells placed at the bottom of the left column. Sensor signals were digitalized by a PCM-DAS16D/16 data acquisition board and processed by HP VEE 5.0 software [25].

Table 1
Characteristics of real acceleration records.

Earthquake	Station	Record Component	Date	PGA (g)	Spectral Displ. (m)
Coalinga, USA	36412 Parkfield- Cholame	000	1983/05/02	0.047	0.0217
Duzce, Turkey	1059 Lamont 1059	000	1999/11/12	0.147	0.0219
Friuli, Italy	8004 Codroipo	270	1976/05/06	0.090	0.0202
Hollister, USA	47189 SAGO South - Surface	295	1986/01/26	0.090	0.0248
Imperial Valley, USA	5169 Westmorland Fire Station	180	1979/10/16	0.171	0.0169
Kobe, Japan	0 MZH	090	2005/01/16	0.052	0.0190
Kocaeli, Turkey	Botas	000	1999/08/17	0.103	0.0262
Landers, USA	12026 Indio - Coachella Canal	000	1992/06/28	0.104	0.0218
Victoria, Mexico	6619 SAHOP Casa Flores	010	1980/06/09	0.101	0.0224
San Fernando, USA	80053 Pasadena - CIT Athenaeum	090	1971/02/09	0.110	0.0253

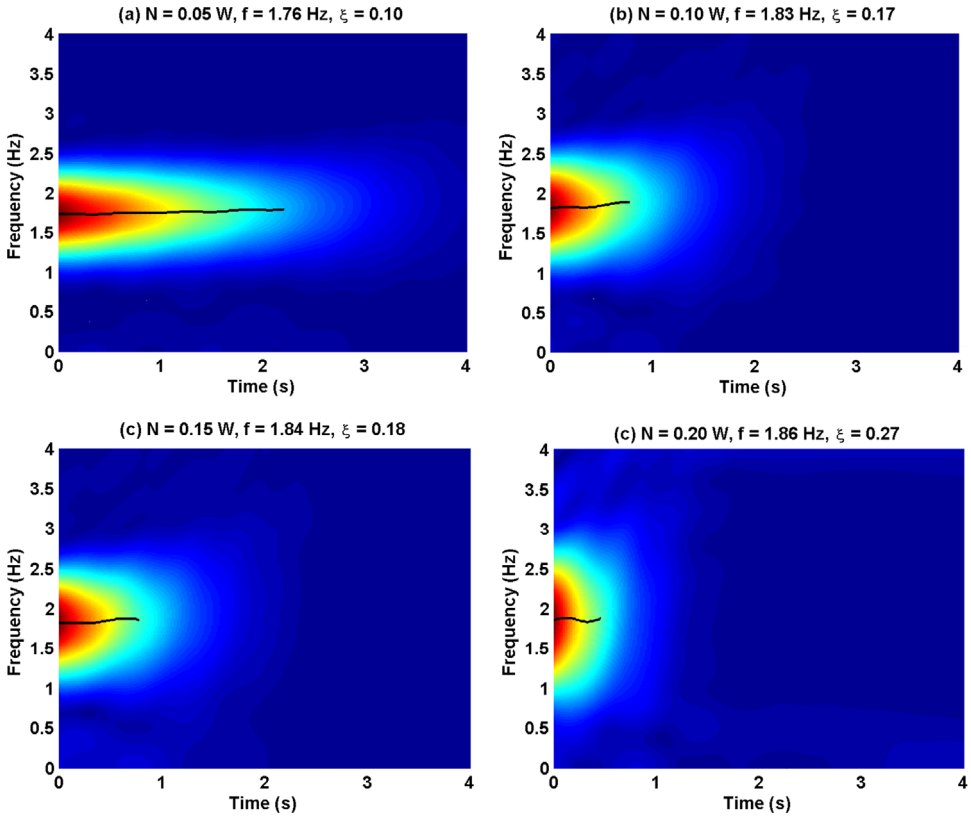

Fig. 5. Fourier spectra of displacement time history from free vibration tests.

3.3. Excitation

In order to draw general conclusions about the seismic performance of building structures provided with the MFD, a set of 10 widely different acceleration records with spectral displacements at 1.74 Hz close to 0.025 m (displacement at elastic limit of the structure) was used in the study. Table 1 shows the characteristics of each real acceleration record.

4. Tests results

4.1. Free vibration tests

To assess the dependence of dynamical parameters of the experimental model provided with MFD on the normal force, free vibration tests were performed. Changes in the fundamental frequency were estimated from spectrograms obtained by applying the short-time Fourier transform on each displacement record measured on the upper beam from initial prescribed

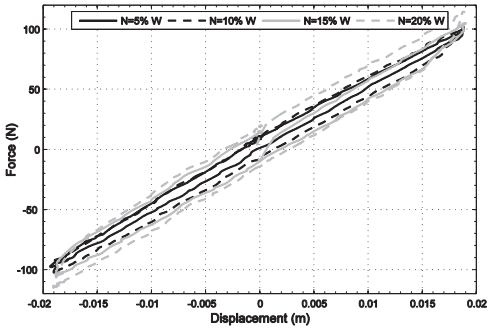

Fig. 6. Hysteresis loop for each case of normal force.

displacement equal to 0.015 m. In order to be able to compare the amplitude decay rate of each case, an equivalent viscous-damping ratio was estimated using the logarithmic decrement method [26]. Fig. 5 shows the spectrogram, the average frequency, *f*, obtained over the ridge of the spectrogram (black line) and the equivalent viscous-damping ratio, ξ, corresponding to each level of normal force. It is worth noting that an increase in the normal force produces a small increase in the effective fundamental frequency and consequently in the effective stiffness of the system, but an important increase in the equivalent viscous damping. Thus, the vibration reduction is principally attributable to energy dissipation.

4.2. Hysteresis loops

Fig. 6 shows hysteresis loops reproduced from force and displacement measurements taken on the upper beam during pseudo-static tests for each normal force. As expected, greater normal force led to greater hysteresis cycle area, indicating greater energy dissipation.

4.3. Forced vibration tests

To demonstrate quantitatively the effectiveness of the proposed MFD to control the structural response, in Table 2 the reduction of dynamical response in terms of maximum and rms (root mean square) values of displacements and accelerations measured on the upper beam are shown for each excitation record and normal force level.

It is observed that, by using a MFD with a normal force equal to N = 0.20 W, the maximum displacement and acceleration may be reduced up to 82% and 66% respectively. Additional reduction is achieved in the rms values. As expected the greater normal force is applied, the further reduction in the structural response is obtained. As mentioned before, the normal force must not exceed the limit in which the MFD might reach stick phase.

As representative examples of forced vibration tests, Figs. 7 and 8 show displacement and acceleration time history records measured on the upper beam with and without MFD under Imperial Valley and Kobe earthquakes. A significant reduction in the maximum and rms values of displacement and acceleration is clearly appreciated.

5. Numerical model and parameter calibration

In order to assess the dynamical behaviour of structures provided with the MFD through numerical simulations, a mathematical model representing the characteristic of the MFD is required. Bouc [27] suggested a versatile, smoothly varying hysteresis model for a single-degree-of-freedom (SDOF) mechanical system (Fig. 9). Later, Wen [28] generalized the Bouc's hysteresis constitutive law and demonstrated that from an appropriate combination of parameters, the model is able to capture, via a differential equation, the behaviour of different hysteretic systems. Because of its versatility and mathematical tractability, the Bouc–Wen model became very popular [29–32] and has been adopted in this study to represent the behaviour of the experimental model provided with the MFD.

The equation of motion of the SDOF system shown in Fig. 9 can be written as:

$$m\,\ddot{u}(t) + c\,\dot{u}(t) + R\big(u(t)\ , z(t), t\big) = F(t) \tag{1}$$

in which u is the displacement of the upper girder, m is the upper girder mass, $F(t)$ is the excitation function; c is the internal damping coefficient determined from the critical damping ratio estimated from free vibration tests and the nonlinear restoring force $R\big(u(t)\ , z(t), t\big)$ provided by the structure stiffness and the friction damper is given by:

$$R\big(u(t)\ , z(t), t\big) = k\,u + \mu_{ef}\ \mathrm{N}z \tag{2}$$

in which k is the stiffness of the structure calibrated from the measured fundamental frequency, μ_{ef} is the identified effective friction coefficient of MFD, N is the measured normal force applied on the friction damper and z is a non-dimensional

Table 2
Reduction of structural response.

Earthquake	Normal Force	Max. Displ. (m)	Reduction Max displ. (%)	Rms Displ. (m)	Reduction Rms displ. (%)	Max. Accel. (m/s²)	Reduction Max accel. (%)	Rms Accel. (m/s²)	Reduction Rms accel. (%)
Coalinga	W/O MFD	0.0172	–	0.0049	–	2.1232	–	0.3512	–
	N=0.05 W	0.0092	−46.51	0.0016	−67.35	1.3345	−37.15	0.1371	−60.96
	N=0.10 W	0.0056	−67.44	0.0011	−77.55	0.9361	−55.91	0.1127	−67.91
	N=0.15 W	0.0047	−72.67	7.69E-04	−84.31	0.9209	−56.63	0.1068	−69.59
	N=0.20 W	0.0036	−79.07	6.35E-04	−87.04	0.7535	−64.51	0.1076	−69.36
Duzce	W/O MFD	0.016	–	0.0038	–	1.9883	–	0.3112	–
	N=0.05 W	0.009	−43.75	0.0013	−65.79	1.2921	−35.01	0.1339	−56.97
	N=0.10 W	0.0057	−64.38	0.001	−73.68	1.0174	−48.83	0.1237	−60.25
	N=0.15 W	0.0051	−68.13	8.75E-04	−76.97	0.873	−56.09	0.1252	−59.77
	N=0.20 W	0.004	−75.00	7.64E-04	−79.90	0.8264	−58.44	0.1371	−55.94
Friuli	W/O MFD	0.0172	–	0.0054	–	2.058	–	0.4332	–
	N=0.05 W	0.0069	−59.88	0.0015	−72.22	0.9626	−53.23	0.145	−66.53
	N=0.10 W	0.0062	−63.95	0.0011	−79.63	1.0231	−50.29	0.1308	−69.81
	N=0.15 W	0.0063	−63.37	8.63E-04	−84.01	1.1056	−46.28	0.1263	−70.84
	N=0.20 W	0.005	−70.93	6.98E-04	−87.08	0.9873	−52.03	0.1237	−71.45
Hollister	W/O MFD	0.0203	–	0.0043	–	2.3845	–	0.3395	–
	N=0.05 W	0.0066	−67.49	0.0011	−74.42	0.9874	−58.59	0.1084	−68.07
	N=0.10 W	0.0048	−76.35	6.42E-04	−85.08	0.7878	−66.96	0.0822	−75.79
	N=0.15 W	0.0043	−78.82	5.12E-04	−88.10	0.8287	−65.25	0.0848	−75.02
	N=0.20 W	0.0038	−81.28	4.31E-04	−89.98	0.8016	−66.38	0.0797	−76.52
Imperial Valley	W/O MFD	0.0164	–	0.0039	–	1.9	–	0.314	–
	N=0.05 W	0.012	−26.83	0.0013	−66.67	1.5529	−18.27	0.1206	−61.59
	N=0.10 W	0.0086	−47.56	9.02E-04	−76.86	1.2303	−35.25	0.1036	−67.01
	N=0.15 W	0.0064	−60.98	7.20E-04	−81.54	1.1427	−39.86	0.105	−66.56
	N=0.20 W	0.0046	−71.95	5.78E-04	−85.18	0.9368	−50.69	0.11	−64.97
Kobe	W/O MFD	0.0184	–	0.0046	–	2.1883	–	0.5103	–
	N=0.05 W	0.0115	−37.50	0.0015	−67.39	1.5609	−28.67	0.1934	−62.10
	N=0.10 W	0.0088	−52.17	0.001	−78.26	1.3051	−40.36	0.1568	−69.27
	N=0.15 W	0.0056	−69.57	6.23E-04	−86.46	1.0228	−53.26	0.1214	−76.21
	N=0.20 W	0.0032	−82.61	3.56E-04	−92.26	0.7462	−65.90	0.1017	−80.07
Kocaeli	W/O MFD	0.0204	–	0.0039	–	2.4046	–	0.3957	–
	N=0.05 W	0.0121	−40.69	0.0013	−66.67	1.5852	−34.08	0.1576	−60.17
	N=0.10 W	0.0095	−53.43	8.75E-04	−77.57	1.3803	−42.60	0.127	−67.90
	N=0.15 W	0.0085	−58.33	6.34E-04	−83.75	1.3896	−42.21	0.1161	−70.66
	N=0.20 W	0.0073	−64.22	5.04E-04	−87.07	1.2802	−46.76	0.1195	−69.80
Landers	W/O MFD	0.0204	–	0.0046	–	2.4506	–	0.4486	–
	N=0.05 W	0.0141	−30.88	0.0018	−60.87	1.7755	−27.55	0.202	−54.97
	N=0.10 W	0.0104	−49.02	0.0014	−69.57	1.4591	−40.46	0.1904	−57.56
	N=0.15 W	0.0085	−58.33	0.0011	−76.09	1.4288	−41.70	0.1808	−59.70
	N=0.20 W	0.0064	−68.63	9.12E-04	−80.18	1.1644	−52.49	0.1807	−59.72
México	W/O MFD	0.0159	–	0.0075	–	1.9248	–	0.4493	–
	N=0.05 W	0.0089	−44.03	0.0026	−65.33	1.1889	−38.23	0.153	−65.95
	N=0.10 W	0.0068	−57.23	0.0017	−77.33	1.0774	−44.03	0.1213	−73.00
	N=0.15 W	0.0057	−64.15	0.0012	−84.00	1.0266	−46.66	0.1091	−75.72
	N=0.20 W	0.0044	−72.33	9.27E-04	−87.64	0.8768	−54.45	0.1061	−76.39
SanFernando	W/O MFD	0.0154	–	0.0049	–	1.9446	–	0.3327	–
	N=0.05 W	0.0136	−11.69	0.0029	−40.82	1.7492	−10.05	0.2161	−35.05
	N=0.10 W	0.0116	−24.68	0.0021	−57.14	1.6957	−12.80	0.1841	−44.66
	N=0.15 W	0.0113	−26.62	0.0018	−63.27	1.7102	−12.05	0.1735	−47.85
	N=0.20 W	0.0102	−33.77	0.0015	−69.39	1.6432	−15.50	0.163	−51.01

evolutionary variable satisfying the following nonlinear first-order differential equation [28]:

$$\dot{z} = x_y^{-1}\left(A\dot{u} - \gamma|\dot{u}|z\,|z|^{\eta-1} - \beta\dot{u}\,|z|^{\eta}\right) \tag{3}$$

in which $A=1,\gamma=\beta=0.5$ y $\eta=1$ are non-dimensional parameters governing the general shape of hysteresis loop and their values were adopted from [33], x_y is the identified plastic displacement threshold of the friction damper and $\dot{u}$ is the velocity of the upper beam mass. Then, Eq. (1) can be written as:

$$\mathrm{m}\,\ddot{u}(t) + \mathrm{c}\,\dot{u}(t) + \mathrm{k}u(t) + \mu_{\mathrm{ef}}\ \mathrm{N}\ z(t) = F(t) \tag{4}$$

To obtain the numerical response, Eq. (4) is converted into a state space representation and then solved through adaptive Runge-Kutta method of 4th order [34].

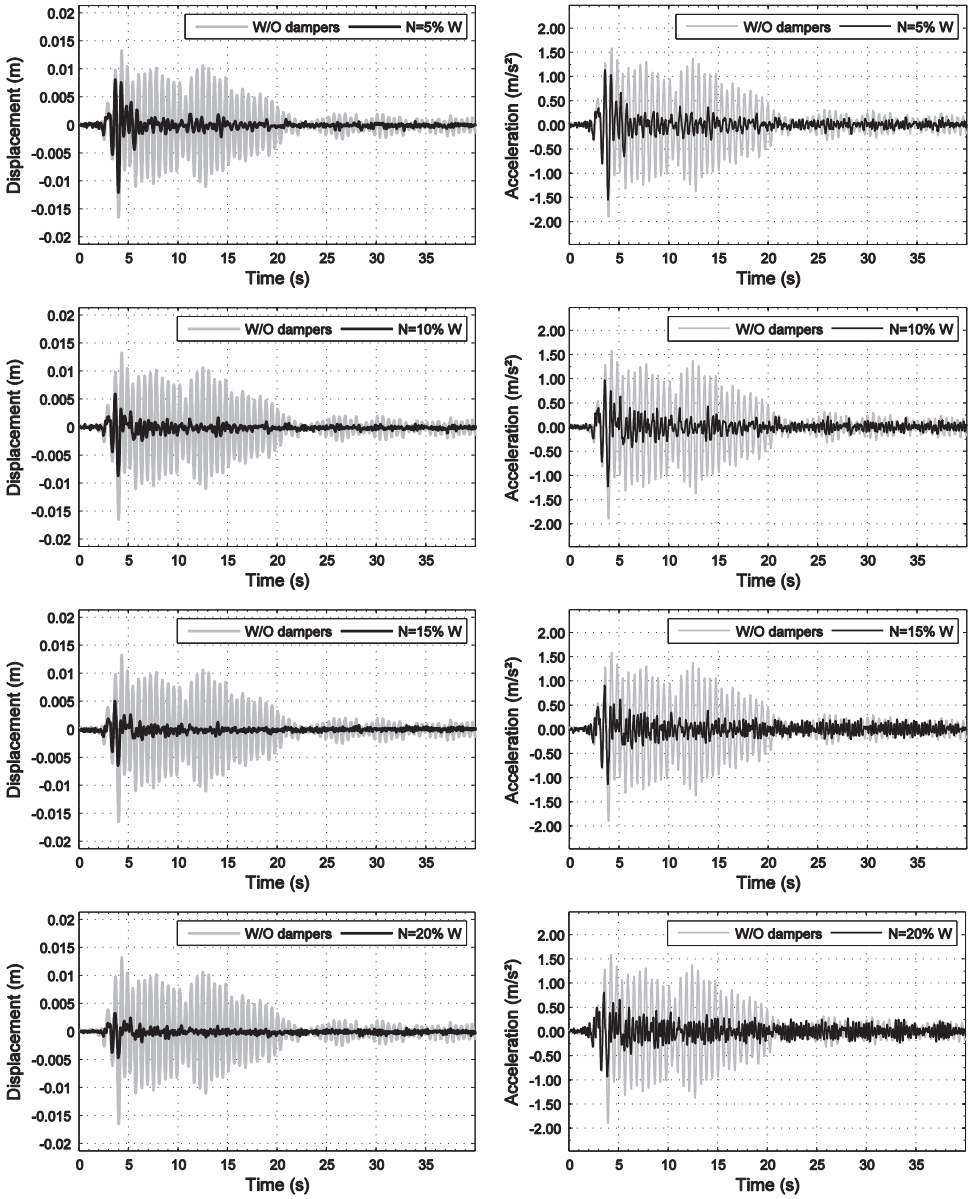

Fig. 7. Displacement and acceleration time history with and without MFD. Imperial Valley earthquake.

5.1. Parameter calibration

Values of the effective friction coefficient, μ_{ef}, and plastic displacement threshold of friction damper, x_y, were identified by fitting the experimental and numerical displacement of the SDOF model in free vibration through the maximization of the Nash-Sutcliffe efficiency coefficient (E). This coefficient is widely used for similarity assessment between physical and numerical time series observations and it is defined as [35]:

$$E = 1 - \frac{\sum_i \left(x_{exp}[t_i] - x_{num}[t_i]\right)^2}{\sum_i \left(x_{exp}[t_i] - \bar{x}_{exp}\right)^2} \tag{5}$$

in which $x_{num}[t_i]$ and $x_{exp}[t_i]$ are the numerical and measured values of the same variable at the instant t_i, respectively, and $\bar{x}_{exp}$ is the mean value of the measured data. Essentially, the closer the efficiency coefficient is to 1, the more accurate the model is.

The estimated parameters, μ_{ef} and x_y, the normalized cross-correlation coefficient (R) [36] and the Nash-Sutcliffe efficiency coefficient (E) for each level of the normal force, N, are shown in Table 3. For all cases, the cross-correlation coefficient

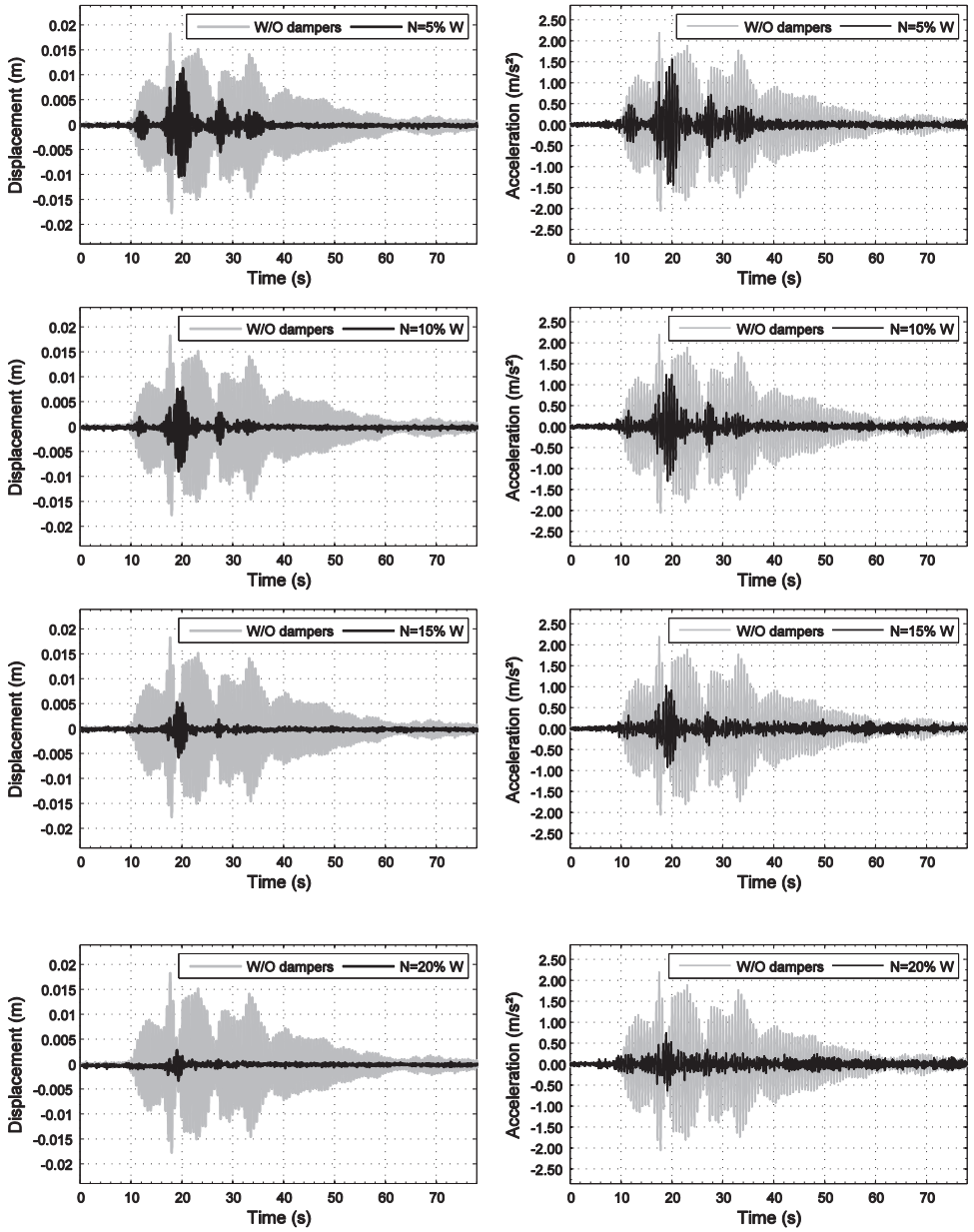

Fig. 8. Displacement and acceleration time history with and without MFD. Kobe earthquake.

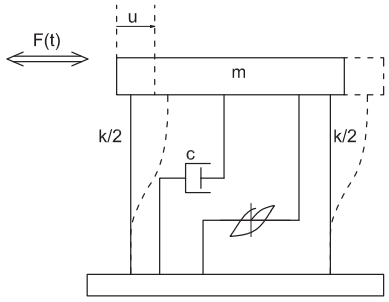

Fig. 9. Schematic SDOF system model.

Table 3
Estimated system parameters.

Normal force (% W)	Friction coefficient μ_{ef}	Displ. threshold x_y (mm)	Cross correlation R	Efficiency coefficient E
5	0.130	1.1	0.97	0.93
10	0.118	1.0	0.97	0.94
15	0.116	1.0	0.96	0.92
20	0.114	1.0	0.99	0.98

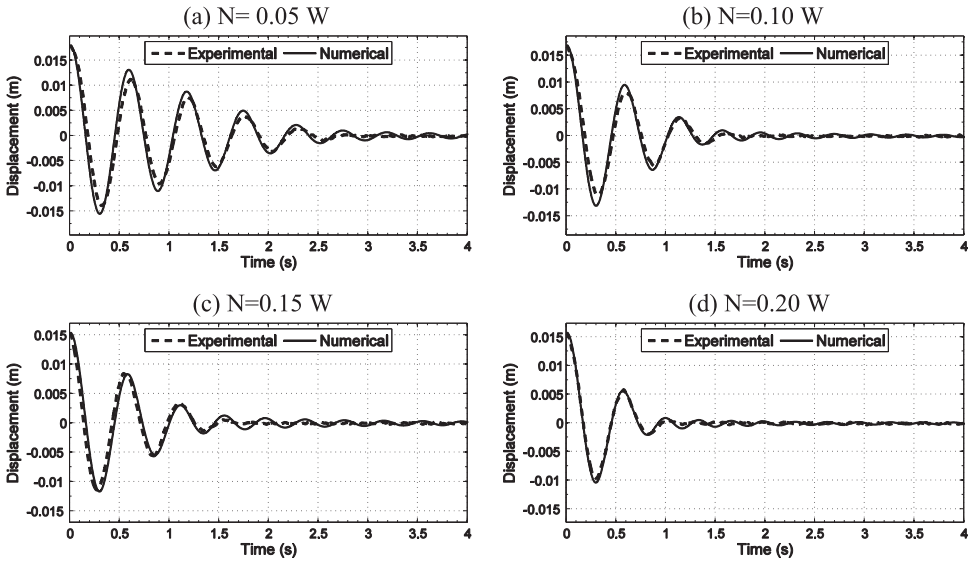

Fig. 10. Free vibration response comparison.

remains above 0.96 and the Nash–Sutcliffe efficiency coefficient above 0.92 demonstrating an excellent similarity between numerical and experimental signals.

Fig. 10 shows a comparison between the experimental and numerical displacement of the system in free vibration for each level of normal force.

5.2. Verification

In order to verify the proposed numerical model, in this section a comparison between experimental and numerical system response in term of hysteretic loops and displacement time history records obtained during forced vibration are presented.

5.2.1. Hysteresis loops

Fig. 11 shows the hysteresis loops numerically reproduced and obtained during pseudo-static tests for each level of normal force.

From the results, it can be inferred that the selected numerical model is suitable to represent the nonlinear behaviour of the structure provided with the proposed MFD.

It is worth noting that, given the difficulties of conducting free vibration test (e.g. large civil structures), the parameter identification (μ_{ef} and x_y,) and subsequent model calibration might be performed through data collected from hysteresis loops reproduced during pseudo-static experimental tests on friction element samples. Then, from Eq. (3) and Eq. (4), the overall system performance can be assessed through simulations.

5.2.2. Forced vibration

In this section, experimental and numerical displacement and acceleration time history records obtained during forced vibration are compared. As representative cases, only are displayed, in Figs. 12 and 13, the responses for Imperial Valley and Kobe earthquakes, respectively. A qualitatively good correlation is observed. For better comparison and visualization, only

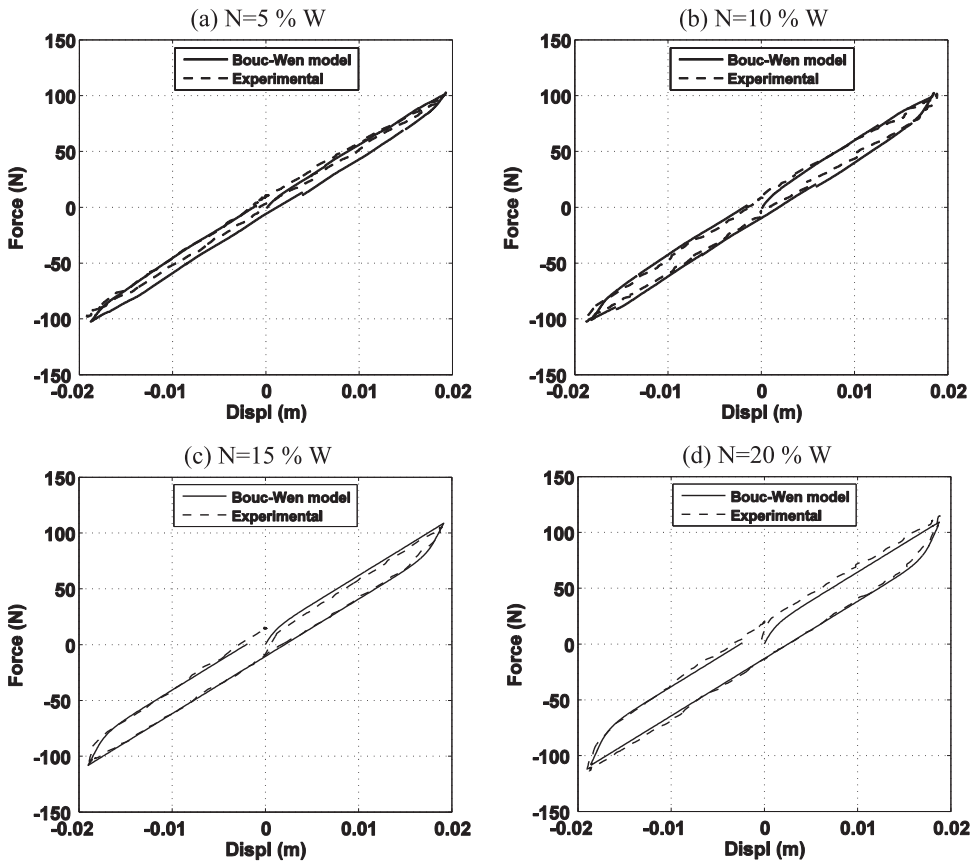

Fig. 11. Hysteresis loops for different applied normal forces.

the significant duration of the records is displayed. Trifunac and Brady [37] define the significant duration of a ground motion record as the time elapsing between the 5% and 95% of the total Arias Intensity. This value represents the period of time at which the greatest amount of energy is provided to the structure by the earthquake.

To quantitatively appreciate the similarity between both time series, maximum values, normalized cross correlation coefficient (R) and Nash-Sutcliffe efficiency coefficient (E) for all cases studied are shown in Table 4.

From Table 4, in general, it can be observed that, the greatest differences between numerical and experimental maximum values occur precisely in the cases which displacements and accelerations are very small right where the measuring errors are greater. The average difference in the maximum values of displacements is 9.6%, while the normalized cross correlation and efficiency coefficient reach average values of 94% and 85%, respectively. The corresponding values for maximum accelerations are 8%, 90% and 81%, respectively.

These results demonstrate that, the accuracy of the numerical model is acceptable for describing the nonlinear behaviour.

6. Conclusions

This article presents a conceptual development of a novel energy dissipation device called Multiple Friction Damper (MFD). This device, unlike traditional friction dampers that are installed using diagonal braces, can be installed on any column without requiring major structural modifications.

Experimental and numerical studies on a reduced experimental model, clearly demonstrated that the new MFD constitutes an effective and reliable alternative to control the response, in terms of displacements and accelerations, of structures under seismic excitation.

Simulation results showed that the suggested numerical model has enough accurate for modelling purposes.

Further research on the technological development of a Multiple Friction Damper prototype and its effectiveness in the structural response control of full scale structures is being carried out.

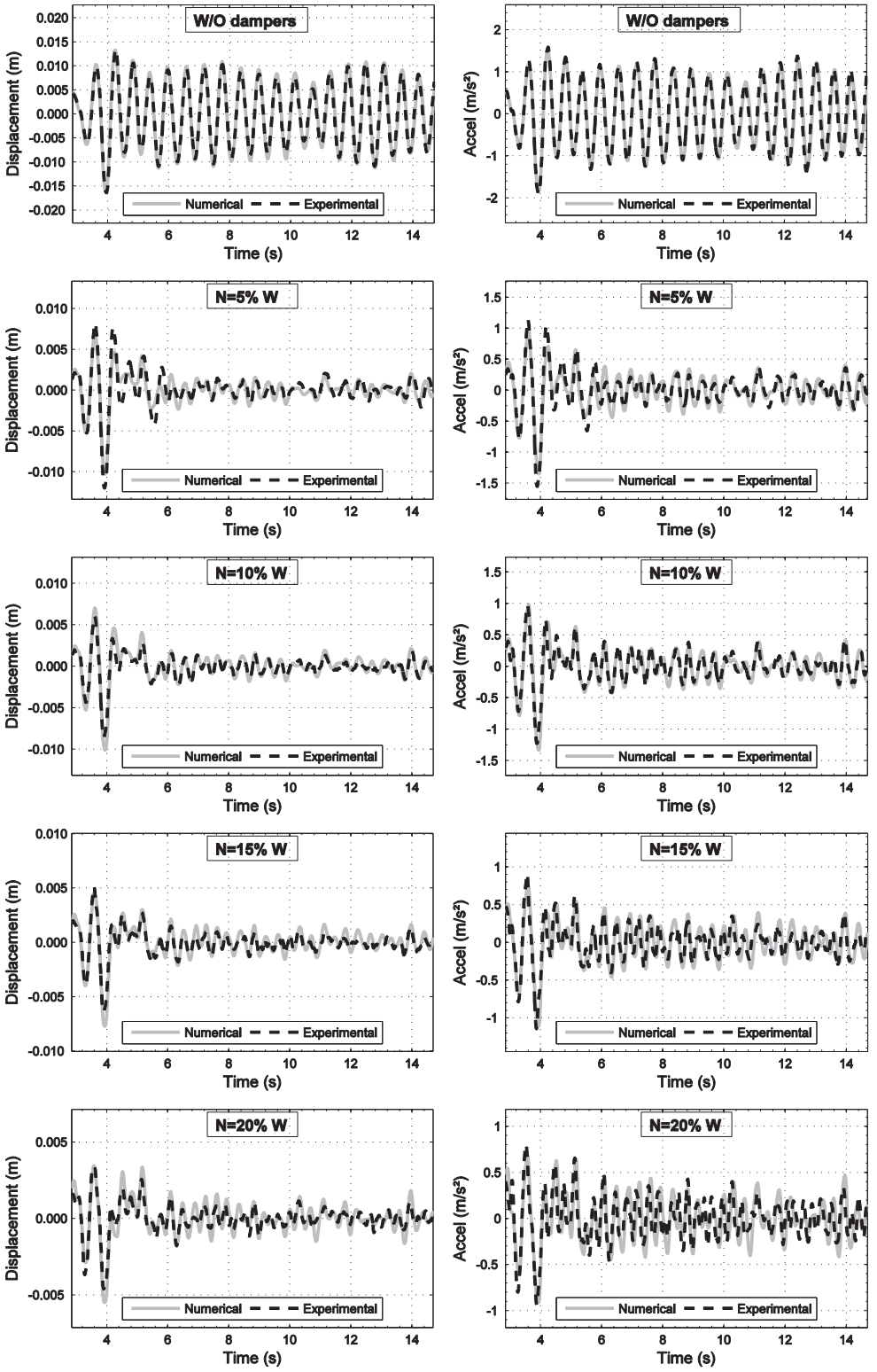

Fig. 12. Displacement and acceleration time history records. Imperial Valley earthquake.

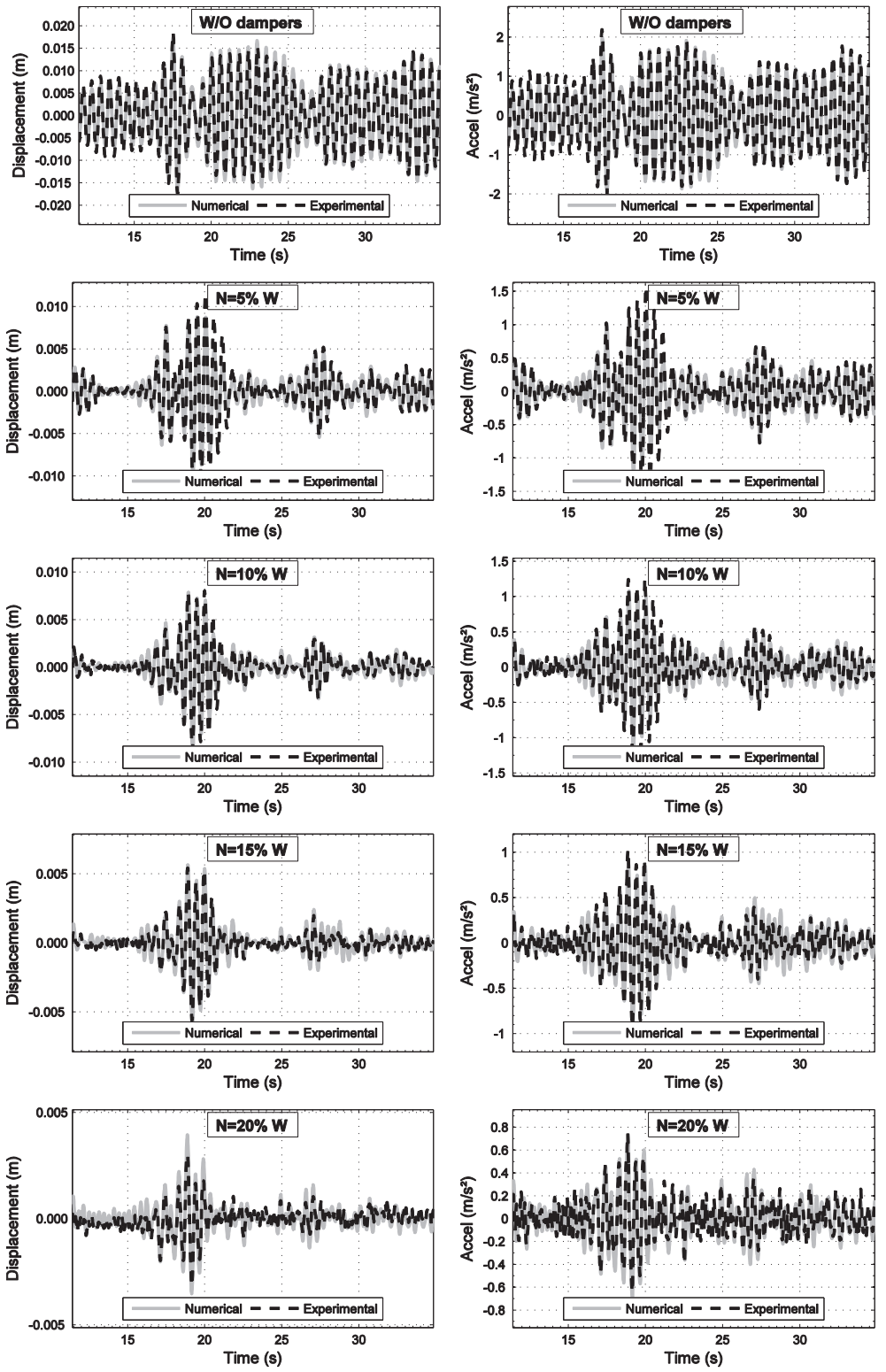

Fig. 13. Displacement and acceleration time history records. Kobe earthquake.

Table 4
Numerical and experimental displacement and acceleration comparison.

Earth-quake	Case	Max displacement					Max acceleration				
		Num. (m)	Exp. (m)	Diff (%)	Cross Corr (R)	Eff. Coeff (E)	Num. (m/s²)	Exp. (m/s²)	Diff (%)	Cross Corr (R)	Eff. Coeff (E)
Coalinga	W/O MFD	0.0183	0.0172	6.40	0.95	0,86	1,3365	1,2303	−1,76	0,98	0,95
	N=0.05 W	0.0096	0.0092	4.35	0.92	0,83	1,111	1,1427	−8,59	0,88	0,77
	N=0.10 W	0.0055	0.0056	−1.79	0.96	0,92	0,911	0,9368	−13,39	0,92	0,84
	N=0.15 W	0.0051	0.0047	8.51	0.93	0,81	1,9835	2,1883	−12,46	0,88	0,75
	N=0.20 W	0.0042	0.0036	16.67	0.93	0,78	1,2576	1,5609	0,74	0,85	0,68
Duzce	W/O MFD	0.0163	0.0160	1.87	0.96	0,95	1,1886	1,3051	−6,30	0,96	0,92
	N=0.05 W	0.0087	0.0090	−3.33	0.95	0,91	0,9232	1,0228	−13,79	0,93	0,87
	N=0.10 W	0.0067	0.0057	17.54	0.95	0,89	0,7338	0,7462	−6,65	0,93	0,87
	N=0.15 W	0.0055	0.0051	7.84	0.94	0,85	2,2107	2,4046	−1,45	0,93	0,85
	N=0.20 W	0.0038	0.0040	−5.00	0.95	0,88	1,3394	1,5852	−13,00	0,91	0,83
Friuli	W/O MFD	0.0182	0.0172	5.81	0.97	0,93	1,1857	1,3803	1,26	0,98	0,95
	N=0.05 W	0.008	0.0069	15.94	0.97	0,93	1,1575	1,3896	8,37	0,94	0,88
	N=0.10 W	0.0071	0.0062	14.52	0.95	0,84	1,185	1,2802	−2,87	0,93	0,84
	N=0.15 W	0.007	0.0063	11.11	0.93	0,77	2,6767	2,4506	−7,35	0,89	0,75
	N=0.20 W	0.0063	0.0050	26.00	0.93	0,74	1,7031	1,7755	1,30	0,85	0,66
Hollister	W/O MFD	0.0205	0.0203	0.99	0.93	0,85	1,3826	1,4591	−1,76	0,96	0,92
	N=0.05 W	0.0079	0.0066	19.70	0.97	0,91	1,2891	1,4288	4,47	0,93	0,85
	N=0.10 W	0.0055	0.0048	14.58	0.96	0,88	1,0909	1,1644	2,39	0,94	0,87
	N=0.15 W	0.0038	0.0043	−11.63	0.92	0,83	1,7056	1,9248	−20,49	0,91	0,82
	N=0.20 W	0.0039	0.0038	2.63	0.95	0,86	1,1257	1,1889	−10,54	0,85	0,68
Imperial Valley	W/O MFD	0.0162	0.0164	−1.22	0.99	0,97	1,0071	1,0774	−2,42	0,97	0,95
	N=0.05 W	0.013	0.0120	8.33	0.95	0,88	0,9234	1,0266	3,47	0,90	0,80
	N=0.10 W	0.0101	0.0086	17.44	0.96	0,85	0,9212	0,8768	8,63	0,93	0,82
	N=0.15 W	0.0077	0.0064	20.31	0.95	0,83	2	1,9446	−2,77	0,85	0,65
	N=0.20 W	0.0055	0.0046	19.57	0.91	0,72	1,5145	1,7492	−2,75	0,75	0,46
Kobe	W/O MFD	0.0174	0.0184	−5.43	0.95	0,92	1,4308	1,6957	−9,36	0,97	0,95
	N=0.05 W	0.0099	0.0115	−13.91	0.94	0,88	1,422	1,7102	−19,43	0,92	0,84
	N=0.10 W	0.0089	0.0088	1.13	0.92	0,85	1,4876	1,6432	−8,93	0,88	0,77
	N=0.15 W	0.0061	0.0056	8.93	0.92	0,80	1,3365	1,2303	−9,74	0,87	0,73
	N=0.20 W	0.0039	0.0032	21.88	0.88	0,59	1,111	1,1427	−1,66	0,82	0,56
Kocaeli	W/O MFD	0.0193	0.0204	−5.39	0.89	0,75	0,911	0,9368	−8,06	0,91	0,82
	N=0.05 W	0.0106	0.0121	−12.40	0.92	0,85	1,9835	2,1883	−15,51	0,86	0,75
	N=0.10 W	0.0088	0.0095	−7.37	0.89	0,76	1,2576	1,5609	−14,10	0,80	0,58
	N=0.15 W	0.0081	0.0085	−4.71	0.88	0,69	1,1886	1,3051	−16,70	0,72	0,37
	N=0.20 W	0.0079	0.0073	8.22	0.89	0,69	0,9232	1,0228	−7,44	0,69	0,34
Landers	W/O MFD	0.0234	0.0204	14.71	0.94	0,86	0,7338	0,7462	9,23	0,92	0,85
	N=0.05 W	0.0138	0.0141	−2.13	0.97	0,93	2,2107	2,4046	−4,08	0,95	0,90
	N=0.10 W	0.0105	0.0104	0.96	0.95	0,88	1,3394	1,5852	−5,24	0,93	0,86
	N=0.15 W	0.0093	0.0085	9.41	0.93	0,83	1,1857	1,3803	−9,78	0,89	0,77
	N=0.20 W	0.0071	0.0064	10.94	0.91	0,76	1,1575	1,3896	−6,31	0,84	0,66
Mexico	W/O MFD	0.0149	0.0159	−6.29	0.99	0,98	1,185	1,2802	−11,39	0,99	0,98
	N=0.05 W	0.0087	0.0089	−2.25	0.95	0,90	2,6767	2,4506	−5,32	0,92	0,85
	N=0.10 W	0.0072	0.0068	5.88	0.96	0,90	1,7031	1,7755	−6,52	0,94	0,88
	N=0.15 W	0.0061	0.0057	7.02	0.97	0,92	1,3826	1,4591	−10,05	0,94	0,88
	N=0.20 W	0.0056	0.0044	27.27	0.94	0,76	1,2891	1,4288	5,06	0,85	0,67
San Fernando	W/O MFD	0.0175	0.0154	13.64	0.97	0,92	1,0909	1,1644	2,85	0,98	0,97
	N=0.05 W	0.0122	0.0136	−10.29	0.95	0,90	1,7056	1,9248	−13,42	0,93	0,86
	N=0.10 W	0.0109	0.0116	−6.03	0.95	0,90	1,1257	1,1889	−15,62	0,93	0,86
	N=0.15 W	0.0105	0.0113	−7.08	0.95	0,89	1,0071	1,0774	−16,85	0,94	0,88
	N=0.20 W	0.0106	0.0102	3.92	0.95	0,87	0,9234	1,0266	−9,47	0,91	0,83

Acknowledgements

The authors gratefully acknowledge the financial support of CONICET and National University of Cuyo. Tests were conducted at the Laboratory of Experimental Dynamics, Institute of Structural Mechanics and Seismic Risk (IMERIS), National University of Cuyo, Argentina.

References

[1] T.T. Soong, G.F. Dargush, Passive Energy Dissipation Systems in Structural Engineering, John Wiley & Sons, New York, 1997.
[2] A.S. Pall, C. Marsh, Response of friction damped braced frames, J. Struct. Eng. ASCE 108 (1982) 1313–1323.

[3] G. Anagnostides, A.C. Hargreaves, T.A. Wyatt, Development and applications of energy absorption devices based on friction, J. Constr. Steel Res. 13 (1989) 317–336, http://dx.doi.org/10.1016/0143-974X(89)90034-5.
[4] T.F. Fitzgerald, T. Anagnos, M. Goodson, T. Zsutty, Slotted bolted connections in a seismic design of concentrically braced connections, Earthq. Spectra 5 (2) (1989) 383–391, http://dx.doi.org/10.1193/1.1585528.
[5] C.E. Grigorian, T.S. Yang, E.P. Popov, Slotted bolted connection energy dissipators, Earthq. Spectra 9 (3) (1993) 491–504, http://dx.doi.org/10.1193/1.1585726.
[6] I. Aiken, S. Kelly, Earthquake simulator testing and analytical studies of two energy absorbing systems for multi-storey structures, Report No. UCB/EERC-90/03, EERC, Berkeley, 1990.
[7] W.Y. Loo, P. Quenneville, N. Chow, A new type of symmetric slip-friction connector, J. Constr. Steel Res. 94 (2014) 11–22, http://dx.doi.org/10.1016/j.jcsr.2013.11.005.
[8] D.K. Nims, P.J. Richter, R.E. Bachman, The use of the energy dissipation restraint for seismic hazard mitigation, Earthq. Spectra 9 (3) (1993) 467–487, http://dx.doi.org/10.1193/1.1585725.
[9] I.H. Mualla, B. Belev, Performance of steel frames with a new friction damper device under earthquake excitation, Eng. Struct. 24 (2002) 365–371, http://dx.doi.org/10.1016/S0141-0296(01)00102-X.
[10] C.G. Cho, M. Kwon, Development and modeling of a frictional wall damper and its applications in reinforced concrete frame structures, Earthq. Eng. Struct. Dyn. 33 (7) (2004) 821–838, http://dx.doi.org/10.1002/eqe.379.
[11] M. Mirtaheri, A.P. Zandi, S.S. Samadi, H.R. Samani, Numerical and experimental study of hysteretic behavior of cylindrical friction dampers, Eng. Struct. 33 (2011) 3647–3656, http://dx.doi.org/10.1016/j.engstruct.2011.07.029.
[12] H.H. Khoo, C. Clifton, J. Butterworth, G. MacRae, Development of the self-centering sliding hinge joint with friction ring springs, J. Constr. Steel Res. 78 (2012) 201–211, http://dx.doi.org/10.1016/j.jcsr.2012.07.006.
[13] H.S. Monir, K. Zeynali, A modified friction damper for diagonal bracing of structures, J. Constr. Steel Res. 87 (2013) 17–30, http://dx.doi.org/10.1016/j.jcsr.2013.04.004.
[14] H.R. Samani, M. Mirthaeri, A.P. Zandi, Experimental and numerical study of a new adjustable frictional damper, J. Constr. Steel Res. 112 (2015) 354–362, http://dx.doi.org/10.1016/j.jcsr.2015.05.019.
[15] A. Filiatrault, S. Cherry, Seismic design spectra for friction damped structures, J. Struct. Eng. ASCE 116 (ST5) (1990) 1334–1355, http://dx.doi.org/10.1061/(ASCE)0733.
[16] S.H. Lee, J.H. Park, S.K. Lee, K.W. Min, Allocation and slip load of friction dampers for a seismically excited building structure based on storey shear force distribution, Eng. Struct. 30 (2008) 930–940, http://dx.doi.org/10.1016/j.engstruct.2007.03.020.
[17] A.V. Bhaskararao, R.S. Jangid, Harmonic response of adjacent structures connected with a friction damper, J. Sound Vib. 292 (2006) 710–725, http://dx.doi.org/10.1016/j.jsv.2005.08.029.
[18] J.H. Park, K.W. Min, L. Chung, S.K. Lee, H.S. Kim, B.W. Moon, Equivalent linearization of a friction damper–brace system based on the probability distribution of the extremal displacement, Eng. Struct. 29 (2007) 1226–1237, http://dx.doi.org/10.1016/j.engstruct.2006.07.025.
[19] Kyung-Won Min, Ji-Young Seong, Jinkoo Kim, Simple design procedure of a friction damper for reducing seismic responses of a single-story structure, Eng. Struct. 32 (2010) 3539–3547, http://dx.doi.org/10.1016/j.engstruct.2010.07.022.
[20] C.A. Martinez, O. Curadelli, M.E. Compagnoni, Optimal design of passive viscous damping systems for buildings under seismic excitation, J. Constr. Steel Res. 90 (2013) 253–264, http://dx.doi.org/10.1016/j.jcsr.2013.08.005.
[21] C.A. Martinez, O. Curadelli, M.E. Compagnoni, Optimal placement of nonlinear hysteretic dampers on planar structures under seismic excitation, Eng. Struct. 65 (2014) 89–98, http://dx.doi.org/10.1016/j.engstruct.2014.01.030.
[22] N. Fallah, S. Honarparast, NSGA-II based multi-objective optimization in design of Pall friction dampers, J. Constr. Steel Res. 89 (2013) 75–85, http://dx.doi.org/10.1016/j.jcsr.2013.06.008.
[23] S. Mirzabagheri, M. Sanati, A.A. Aghakouchaka, S.E. Khademb, Experimental and numerical investigation of rotational friction dampers with multi units in steel frames subjected to lateral excitation, Arch. Civil. Mech. Eng. 15 (2) (2015) 479–491, http://dx.doi.org/10.1016/j.acme.2014.05.009.
[24] M. Krack, S. Tatzko, L. Panning-vonScheidt, J. Wallaschek, Reliability optimization of friction-damped systems using nonlinear modes, J. Sound Vib. 333 (2014) 2699–2712, http://dx.doi.org/10.1016/j.jsv.2014.02.008.
[25] H.P. Hewlett Packard, VEE Advanced Programming Techniques, Hewlett-Packard Company, Palo Alto, California, 1998.
[26] R.W. Clough, J. Penzien, Dynamics of Structures, 2nd ed, Mc-GrawHill, New York, 1993.
[27] R. Bouc, Forced vibration of mechanical systems with hysteresis, in: Proceedings of the Fourth Conference on Nonlinear Oscillation. Prague, Czechoslovakiapp. 315, 1967.
[28] Y.K. Wen, Method for random vibration of hysteretic systems, J. Eng. Mech. ASCE 102 (1976) 249–263.
[29] G.Z. Yao, F.F. Yap, G. Chen, W.H. Li, S.H. Yeo, MR damper and its application for semi-active control of vehicle suspension system, Mechatronics 12 (7) (2002) 963–973, http://dx.doi.org/10.1016/S0957-4158(01)00032-0.
[30] N.M. Kwok, Q.P. Ha, M.T. Nguyen, J. Li, B. Samali, Bouc–Wen model parameter identification for a MR fluid damper using computationally efficient GA, ISA Trans. 46 (2) (2007) 167–179, http://dx.doi.org/10.1016/j.isatra.2006.08.005.
[31] F. Ikhouane, J.E. Hurtado, J. Rodellar, Variation of the hysteresis loop with the Bouc–Wen model parameters, Nonlinear Dyn. 48 (4) (2007) 361–380, http://dx.doi.org/10.1007/s11071-006-9091-3.
[32] M. Ismail, F. Ikhouane, J. Rodellar, The hysteresis Bouc-Wen Model, a survey, Arch. Comput. Methods Eng. 16 (2) (2009) 161–188, http://dx.doi.org/10.1007/s11831-009-9031-8.
[33] F. Ikhouane, J. Rodellar, Systems with Hysteresis. Analysis, Identification and Control using the Bouc–Wen Model, John Wiley & Sons Ltd, Chichester, England, 2007.
[34] D. Inman, Engineering Vibration, 4th ed, Prentice Hall Inc, New Jersey, 2013.
[35] J.E. Nash, J.V. Sutcliffe, River flow forecasting through conceptual models part I- A discussion of principles, J. Hydrol. 10 (3) (1970) 282–290, http://dx.doi.org/10.1016/0022-1694(70)90255-6.
[36] T.A.L. Wren, K.P. Do, S.A. Rethlefsen, B. Healy, Cross-correlation as a method for comparing dynamic electromyography signals during gait, J. Biomech. 39 (2006) 2714–2718, http://dx.doi.org/10.1016/j.jbiomech.2005.09.006.
[37] M.D. Trifunac, A.G. Brady, A study on the duration of strong earthquake ground motion, Bull. Seism. Soc. Am. 65 (1975) 581–626.